

# Common-Path Interferometric Wavefront Sensing for Space Telescopes

J. Kent Wallace  
Jet Propulsion Laboratory/California Institute of Technology  
4800 Oak Grove Dr.  
Pasadena, CA 91109  
818-393-7066  
James.K.Wallace@jpl.nasa.gov

*Abstract*—This paper presents an optical configuration for a common-path phase-shifting interferometric wavefront sensor.<sup>1,2</sup> This sensor has a host of attractive features which make it well suited for space-based adaptive optics. First, it is strictly reflective and therefore operates broadband, second it is common mode and therefore does not suffer from systematic errors (like vibration) that are typical in other interferometers, third it is a phase-shifting interferometer and therefore benefits from both the sensitivity of interferometric sensors as well as the noise rejection afforded by synchronous detection. Unlike the Shack-Hartman wavefront sensor, it has nearly uniform sensitivity to all pupil modes. Optical configuration, theory and simulations for such a system will be discussed along with predicted performance.

## TABLE OF CONTENTS

1. INTRODUCTION.....	1
2. PRINCIPLE OF ZERNIKE PHASE-CONTRAST.....	1
3. PRINCIPLE OF THE PHASE-SHIFTING ZERNKIE WAVEFRONT SENSOR .....	3
4. OPTICAL ARCHITECTURE FOR A REFLECTIVE ZERNIKE WAVEFRONT SENSOR .....	4
5. PERFORMANCE SIMULATIONS .....	5
6. APPLICATIONS OF THE ZERNIKE WAVEFRONT SENSOR ..	5
7. FUTURE WORK .....	6
8. CONCLUSION .....	6
9. ACKNOWLEDGEMENTS .....	6
REFERENCES .....	7
BIOGRAPHY .....	7

## 1. INTRODUCTION

Much information is carried in an electric field's phase. This is somewhat unfortunate because the process of simple imaging (by our eye, with photographic film, pixels in a CCD or any other detector) measures the energy in the electric field. In this process phase information is lost. Many methods have been developed to extract this phase from the electric field. These phase sensors include ronchi tests, interferometers of all types, phase gradient sensors like the Shack-Hartman and knife-edge tests, curvatures sensors, Pyramid WFS. It's a rich area of active research with very broad applicability.

Zernike discovered a particularly elegant method of directly imaging the electric field phase, known as the method of phase-contrast, for which he was awarded the Nobel Prize. Although it found immediate application in microscopy of transparent biological specimens, Dicke realized its potential application to wavefront sensing and control as applied to astronomy.

Here, I extend the principle in several ways. First a relatively simple optical architecture which makes the sensor more practical to implement is shown. Second, a dynamic phase-modulation is presented along with the reconstruction algorithm. Benefits of this new phase sensor are described. And finally, its broad utility is demonstrated by its application to several different phase sensing scenarios.

## 2. PRINCIPLE OF ZERNIKE PHASE-CONTRAST

I start with a short review of the fundamental phase-contrast concept. A description of this can be found in many books and articles [1 – 4]. The development here, however, makes explicit the affect of amplitude variability in the system. The canonical optical system is illustrated in Figure 1.

Light enters the system on the left of the diagram and passes through a screen of spatially varying transmission and phase that is immediately before the input pupil. This field is subsequently focused by a lens to form a point spread function (PSF) in the image plane. An optical element with a phase delay of  $\lambda/4$  within a diameter of a few  $\lambda/D$  is centered on this PSF. After passing through the focal plane element, the light continues to propagate to the output pupil where the optical intensity is measured.

The electric field immediately before the input is given by:

$$E(u, v) = P(u, v) \cdot A(1 + \varepsilon(u, v))e^{i\varphi(u, v)} \quad (1)$$

Here, the pupil function is given by  $P(u, v)$ , the mean electric field amplitude is  $A$ , the point-by-point variation in the electric field strength is given by  $\varepsilon(u, v)$ . The pupil-dependent phase is given by  $\varphi(u, v)$ . For simplicity sake, let's first assume that the phase in the input pupil is small, compared to a radian. With this assumption the expression for the electric field then becomes:

<sup>1</sup>978-1-4244-7351-9/11/\$26.00 ©2011 IEEE.

<sup>2</sup>IEEEAC paper #1527, Version 5, Updated 2011:3:16.

$$\begin{aligned}
E(u, v) &\approx P(u, v) \cdot A(1 + \varepsilon(u, v)(1 + i\varphi(u, v))) \\
E(u, v) &\approx P(u, v) \cdot A(1 + \varepsilon(u, v) + i\varphi(u, v) + i\varepsilon(u, v)\varphi(u, v)) \quad (2) \\
E(u, v) &\approx P(u, v) \cdot A(1 + \varepsilon(u, v) + i\varphi(u, v))
\end{aligned}$$

Here, the second order terms have been dropped. This field is propagated to the focal plane of the system by a Fourier transform. This Fourier transform operator is shown schematically as  $F[\cdot]$ :

$$\begin{aligned}
E(\eta, \nu) &= F[P(u, v)] * F[A(1 + \varepsilon(u, v) + i\varphi(u, v))] \\
E(\eta, \nu) &= A \text{PSF}(\eta, \nu) * \left\{ \delta(\eta, \nu) + F[\varepsilon(u, v) + i\varphi(u, v)] \right\} \\
E(\eta, \nu) &= A \text{PSF}(\eta, \nu) + A \text{PSF}(\eta, \nu) * F[\varepsilon(u, v) + i\varphi(u, v)] \quad (3)
\end{aligned}$$

where the Cartesian coordinates in the image plane are represented by  $\eta, \nu$  and the convolution operation is represented by the  $*$  symbol. The Fourier transform of the pupil function is represented by PSF. The electric field in the image plane is therefore given by the sum of two terms, the first is the PSF of the system with a perfect input field (no phase or amplitude errors). The second term is given by the convolution of this PSF with the Fourier transform of the phase and amplitude errors of the input beam.

Next, a phase shift is applied to the PSF portion of the image plane electric field. In theory, the PSF has infinite extent, so applying a uniform phase-shift to this part of the full extended field appears problematic. However, in

practice, most of the energy of the PSF is located in a very compact area. For typical systems,  $\sim 85\%$  of the energy lies with a diameter of  $\sim 2 \lambda/D$  where  $\lambda$  is the wavelength of operation and  $D$  is the input pupil diameter. Again for simplicity's sake, we will mathematically apply a uniform phase shift to the PSF. In numerical simulations we quantify the error in this assumption (but rest assured, it's a small effect). The magnitude of the phase shift is given by  $\theta$ ,

$$\begin{aligned}
E(\eta, \nu) &= A \text{PSF}(\eta, \nu)e^{i\theta} + A \text{PSF}(\eta, \nu) * F[\varepsilon(u, v) + i\varphi(u, v)] \quad (4)
\end{aligned}$$

Sensing will be done in the pupil plane, so a subsequent Fourier transform is needed to quantify the response in this plane. The Cartesian coordinates are represented by  $(x, y)$  in the re-imaged plane.

$$F[E(\eta, \nu)] = E(x, y) = F \left[ A \text{PSF}(\eta, \nu)e^{i\theta} + A \text{PSF}(\eta, \nu) * F[\varepsilon(u, v) + i\varphi(u, v)] \right]$$

$$E(x, y) = A P(x, y)e^{i\theta} + A P(x, y) \left( \varepsilon(x, y) + i\varphi(x, y) \right)$$

$$E(x, y) = A P(x, y) \cdot (e^{i\theta} + \varepsilon(x, y) + i\varphi(x, y)) \quad (5)$$

The electric field from the original input pupil has been modified in the re-imaged output pupil in following way: the DC part of the electric field has been replaced by its phase-shifted version. This phase shift is nearly uniform across the re-imaged pupil plane. For the sake of brevity, in the next few set of equations the explicit coordinates will be dropped. Likewise, the pupil function will be implied and its explicit notation is also dropped.

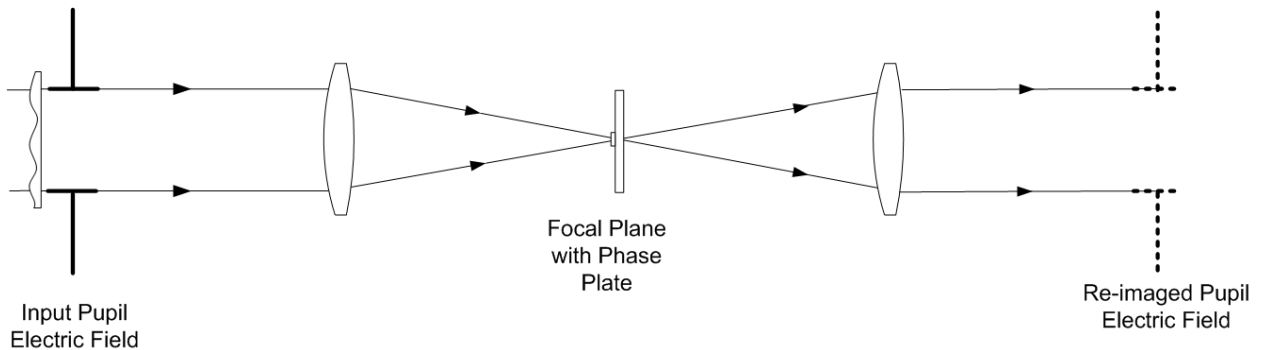


**Figure 1** – Optical layout of canonical optical system to elucidate Zernike phase-contrast. The electric field enters on the left and propagates to the right. It first passes through a transparent phase aberration immediately before the input pupil of the system. A lens then focus the light to a image plane, and a resulting point spread function is centered on a static phase delay of  $+\lambda/4$  whose diameter is roughly a few resolution elements ( $\sim \text{few } \lambda/D$ ). This pupil is then subsequently imaged by a second lens to the output pupil on the right.

With a static phase shift of  $+\lambda/4$  ( $\theta = +\pi/2$ ), the electric field and intensity at the output pupil plane are:

$$E = A\left(e^{+i\pi/2} + \varepsilon + i\varphi\right) = A(i + \varepsilon + i\varphi)$$

$$I = E \cdot E^* = A^2(1 + 2\varphi + \varepsilon^2 + \varphi^2) \quad (6)$$

The intensity in the pupil image given by Eq. 6 above can be characterized as a pedestal that is the mean intensity at the input pupil but modulated by the addition of a few terms. The first term is proportional to twice the phase at that location in the input pupil. The final two terms are proportional to the square of the amplitude and phase errors. With the assumption that  $\varphi < 1$ , then  $\varphi^2 \ll \varphi$  and can be ignored. It is also typically assumed that transmission variability,  $\varepsilon$ , is small compare to phase variability and can likewise be ignored.

There are a few noteworthy benefits to point out. First of these is its elegant simplicity. Any pupil viewing instrument that also has an accessible, intermediate focus can become a sensitive phase measuring device by the addition of the phase mask centered on the PSF. Second, the measurement is easily interpreted. Bright areas are phase bumps above the mean phase, and darker areas are phase troughs. Third, the sensor is common-mode in the sense that after the focal plane mask, the PSF core that has been phase shifted co-propagates with the other parts of the original electric field. After the focal plane mask, the measurement is less affected by phase errors like air turbulence or optical fabrication errors because these affect both co-propagating beams in nearly the same way. Fourth, the sampling is easily changed with the addition of a zoom lens between the pupil and final image plane. Under certain circumstances, it may be beneficial to sample the phase with greater resolution, at the expense of more noise. Fifth, for adaptive optics system that require a phase estimate at high speed, deformable mirror elements and pupil pixel elements can be mapped one-to-one for optimum noise performance. The reconstruction algorithm is extremely simple to implement and can be done on a pixel-by-pixel basis. The benefits of this common-mode interferometric wavefront sensor has been previously noted by others [7].

However, there are some limitations to this static phase offset. Given that it is fundamentally an intensity measurement, any system error that results in a detector signal variation that is not due to phase, will lead to an corresponding incorrect phase estimation. For example, a variable dark current intrinsic to the detector results in signal variations that could be misinterpreted as phase. Likewise, amplitude fluctuations (like atmospheric scintillation) can create spurious signals (albeit as a second order effect). Below we describe an improvement to the sensor that allows us to mitigate against these deleterious effects.

### 3. PRINCIPLE OF THE PHASE-SHIFTING ZERNIKIE WAVEFRONT SENSOR

Many of the detection limitations described above can be removed by introducing a time varying modulation into the phase shift of the Zernike phase sensor. Modulation of the phase shift will, of necessity, create a temporal modulation in the intensity measurement. De-modulation of these intensity measurements results in: 1) a direct measurement of the phase and 2) rejection of many systematic error terms listed above.

Let's consider electric fields and corresponding intensities in the output pupil plane for four different phase steps from  $-\lambda/4$  to  $+\lambda/2$  in steps of  $+\lambda/4$  ( $\theta = -\pi/2, 0, \pi/2, \pi$ ).

$$E_1 = A\left(e^{-i\pi/2} + \varepsilon + i\varphi\right) = A(-i + \varepsilon + i\varphi)$$

$$E_2 = A\left(e^{-i0} + \varepsilon + i\varphi\right) = A(1 + \varepsilon + i\varphi)$$

$$E_3 = A\left(e^{i\pi/2} + \varepsilon + i\varphi\right) = A(i + \varepsilon + i\varphi)$$

$$E_4 = A\left(e^{-i\pi} + \varepsilon + i\varphi\right) = A(-1 + \varepsilon + i\varphi)$$
(7)

The intensity measurements are then:

$$I_1 = E_1 \cdot E_1^* = A^2(1 + \varepsilon^2 - 2\varphi + \varphi^2)$$

$$I_2 = E_2 \cdot E_2^* = A^2(1 + \varepsilon^2 + 2\varepsilon + \varphi^2)$$

$$I_3 = E_3 \cdot E_3^* = A^2(1 + \varepsilon^2 + 2\varphi + \varphi^2)$$

$$I_4 = E_4 \cdot E_4^* = A^2(1 + \varepsilon^2 - 2\varepsilon + \varphi^2)$$
(8)

From these four intensity measurements, the pupil dependent phase and amplitude errors of the electric field at the input pupil can be estimated.

$$\varphi = \frac{I_3 - I_1}{4A^2} \quad (9)$$

$$\varepsilon = \frac{I_2 - I_4}{4A^2} \quad (10)$$

Therefore, a simple difference in the intensity images taken when the phase step is  $-\pi/2$  and  $\pi/2$  provides an estimate of the phase, and similarly the difference images at 0 and  $\pi$  provide the estimate for amplitude errors (both up to second order). Now, there were some simplifying assumptions to reach the expressions above, in particular the assumption that the input phase errors are small. These assumptions are typically well justified. However, I have developed a more robust but deriving it here is outside the

scope of this work, and it takes away from the intuitive and elegant simplicity of Eq. 10.

The introduction of a dynamic phase shift to the nominal PSF gives this sensor a unique advantage over those sensors that use a static phase shift. It allows the reference beam electric field to be modulated at a unique, selectable frequency. The resulting intensity measurements are also modulated at this frequency, and the demodulation process will reject noise that is not at the frequency of the intensity modulation. Phase modulation also rejects those intensity signals that are not either optically incoherent with the reference beam or not synchronous with the reference light phase shift. For instance, intensities that might arise due to background illumination (static or dynamic) or light scattered internal to the sensor will also be rejected.

The benefits of this dynamic phase modulation are evident, and other types of wavefront sensors based upon this technique have been developed [8-13]. However, implementation of the phase shifting has resulted in systems that are not simple to fabricate, are wavelength sensitive, or polarization sensitive. In the next section I describe an

architecture for a phase-shifting Zernike phase sensor that is fundamentally easy to fabricate but also benefits from broadband operation and polarization insensitivity.

#### 4. OPTICAL ARCHITECTURE FOR A REFLECTIVE ZERNIKE WAVEFRONT SENSOR

The diagram of the reflective Zernike phase sensor is shown below in Figure 2. It consists of an input pupil located at the focal length of the parabolic mirror. The light enters through this input pupil plane and reflects from an off-axis portion of a full parabola towards the focal point. Located in the focal plane is a special optical element that is comprised of a end-polished metal wire supported within a ceramic ferrule. The ceramic ferrule has been end polished and coated with the same metal as the filament. The translation of tip of the polished wire with respect to the coated face of the ferrule provides the phase shifting of the PSF core. The light reflects off this assembly and is re-collimated by the parabola. The output pupil image is formed at the focal length of the parabola.

The wire is phase shifted by the PZT. One end PZT is

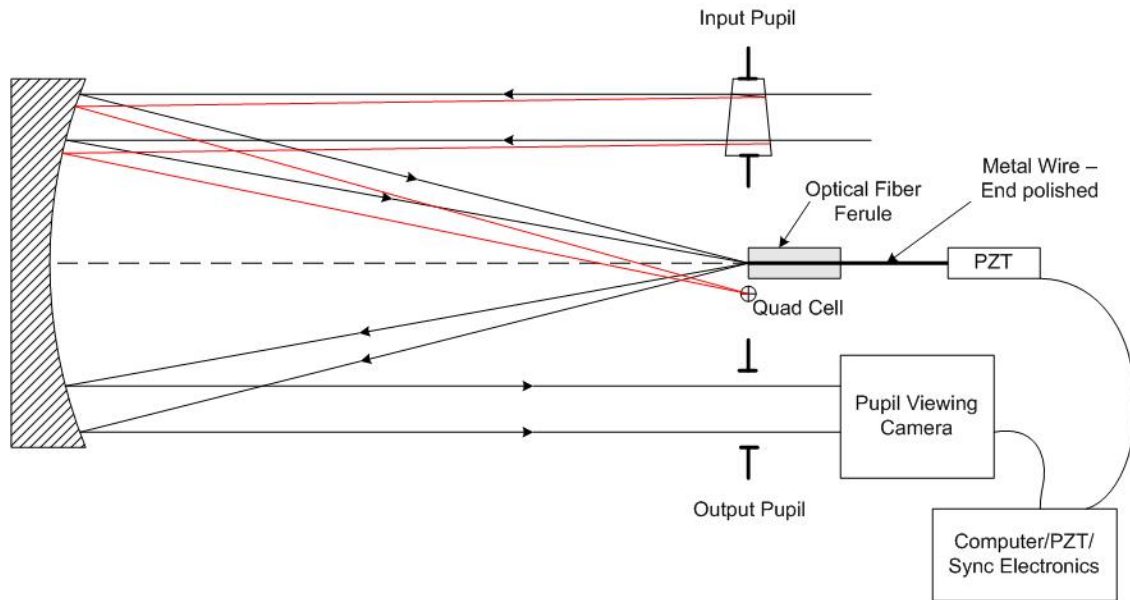


**Figure 2** – Schematic diagram of the reflective Zernike wavefront sensor. The input pupil is in the upper right. Upon reflection from the OAP, the pupil is imaged to infinity, and the PSF is centered on the core of a phase-shifting element. After reflection, a real pupil is formed again at the bottom right and is imaged by a pupil viewing camera.

bonded to the ceramic ferrule, the other is bonded to the wire. The bonding is done such that the polished end is flush with the ferrule face when the PZT is at mid-voltage. This ensures the phase shift has an equal stroke about its nominal position. The typical required stroke of the PZT is on the order of a few wavelengths for segment phasing, and only +/- quarter of a wavelength for typical operation. The PZT stroke and camera frame acquisition can be synchronized with dedicated timing electronics if the requirements is to run fast under circumstances where the phase sensing must be done quickly (like closed-loop adaptive optics systems) Or this synchronization can be done via computer for lab operation.

A dedicated quad cell detector has been added to the system in order to ensure the PSF is well centered on the core of the axis of the ferrule. An out-of-band ghost image created by a judiciously wedged and coated optic at the input pupil provides an optical reference that is locked to the position of the beam under study. The quad cell detector is also physically referenced to the ceramic ferrule, carefully aligned and secured in place. Initial calibration of the pointing is done by retracting the wire into the ferrule such that the reflective ferrule acts as a hard-edged coronagraph. In this configuration, the input PSF is then dithered in a cross-pattern, back and forth, up and down, while synchronous with the output pupil viewing camera. Proper differences of the back/forth and up/down images provides signed error signals that, in closed loop with the input dither mirrors, can center the beam extremely accurately. Once centered in this way, the reference position on the quad cell detector is recorded, and finally, the polished wire is restored to its nominal position

The reflective design makes the architecture insensitive to differential phase effects due to chromaticity and polarization. Incredibly, the only phase difference between the core of the PSF and the remaining portion of the electric field is due to the physical displacement of the polished wire itself. Another nice benefit to this design is that it is entirely common mode. So, even though at its heart it is an interferometer, because the beam co-propagate, they are unaffected by non-common path errors and vibrations that detrimentally impacts the performance of other interferometers.

## 5. PERFORMANCE SIMULATIONS

We have performed numerical simulations to predict the performance of this sensor. These simulations were done using a very efficient Fourier-Transform calculation which implements a semi-analytical approach[14]. Simulations also include the broadband effects by combining several discrete wavelengths. It also captured the effect of the wavelength dependent phase shift for a given physical delay as well as the change in the effective size of the phase-shifted core of the PSF (whose size varies linearly with

wavelength). Here we assumed a broadband source with 20% bandwidth, and a phase shifting core whose size is  $1.5 \lambda/d$  at the center wavelength.

The first of these simulations is shown below in Fig. 3. For this broadband performance simulation, we put in two sinusoidal phase ripples of different frequency and amplitude into the input pupil. In the figure, we show a two dimensional image of the input phase and a slice through the center.

This input phase was then propagated through the optical system for each of the discrete wavelengths for each of the four phase-shifted cores. Broadband intensity images were simply created by summing the resultant output pupil intensities calculated for each wavelength. The results were then four different intensity measurements corresponding to the four phase shifts ( $\theta = -\pi/2, 0, \pi/2, \pi$ ).

The input phase was reconstructed using the reconstruction algorithms of Eqs. 9 and 10. The reconstructed phase is shown in the lower portion of Fig. 3. The two dimensional phase reconstruction in the output pupil and a slice through the middle of the pupil is shown in blue, and overlaid upon the same slice of the phase at the input pupil. As can be seen, there is excellent agreement between the input phase error and the phase that is reconstructed based upon the four intensity measurements and the rather simple reconstruction algorithm.

## 6. APPLICATIONS OF THE ZERNIKE WAVEFRONT SENSOR

Independent of the excellent optical properties, other researchers recognize that the Zernike wavefront sensor also has superior sensitivity to photon noise [15]. Likewise, given the fact that it is also a common-mode coherence sensor, it has been used for the phasing of segmented apertures [16 - 18].

Our wavefront sensor benefits from these properties as well. As a matter of fact, it can easily be configured to run in two different modes: 1) long-stroke mode for phase aberrations with large excursions and 2) small-stroke mode when the aberrations are known to be much smaller than a wavelength. These two modes require a larger stroke on the phase-shifting element, but this is easily accomplished by applying a larger voltage on the PZT element that drives the active element. The small-stroke phase reconstruction algorithm was presented above and is still valid. For the large-stroke algorithm, the fundamental operation is to detect the ‘white-light’ envelope for each pixel in the pupil-viewing camera. This is done by measuring the group delay of each white light fringe that is recorded in each pixel in the pupil viewing camera. This is accomplished by measuring the slope of the imaginary part FFT of each pixels fringe pattern.

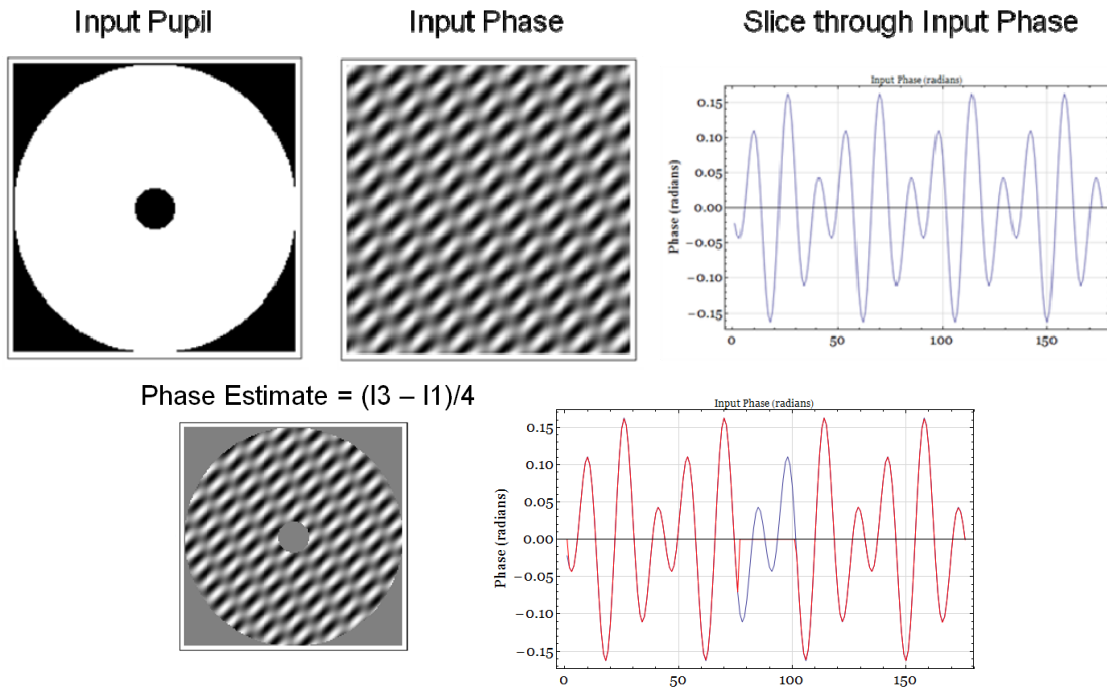


**Figure 3** – Performance simulations of the Zernike wavefront sensor. The input pupil and phase errors are shown in the top row of this figure. The two-dimensional phase map and the slice through the center of this phase map are shown on the top. On the bottom row is the reconstructed phase based upon the four phase-shifted intensity measurements described in the text. The reconstructed phase compares well with the input phase errors as shown by the overlay of the one-dimensional slices.

## 7. FUTURE WORK

We have recently been awarded funds to build and test this wavefront sensor concept in the lab. Our final goal is to implement this wavefront sensor on the Palomar adaptive optics system, and with that in mind our system is designed to work in the visible with a very fast, science-grade, low-noise CCD. Our goals in the first year are to demonstrate the fundamental physics of this sensor. This will require us to first design, specify, order, build the optical system. Then, testing will consist of making an absolute measurement of a known phase aberration. Our aim is to quantify the difference in these measured quantities to less than five nanometers, rms. Once this work is complete, we will then concentrate our efforts on engineering a sensor that is compatible with the adaptive optics system at Palomar Observatory.

## 8. CONCLUSION

An optical architecture for a phase-shifting Zernike wavefront sensor has been presented. This sensor still has the many benefits of a common-mode wavefront sensor (in particular its insensitivity to vibration and air-turbulence). However, it has the additional benefits of: 1) being reflective such that it operates broad-band is completely polarization sensitive 2) phase-shifting. The phase-shifting property allows this sensor to reject the  $1/f$  noise of the detector and also reject noise due to stray light.

Our work plan is to first demonstrate the fundamental physics of this sensor in the lab during the first year. Our goal will be to understand its absolute phase measuring accuracy at the few nanometer (rms) level in the visible. After this, we will use our knowledge gained in the lab to build a wavefront sensor the adaptive optics system at Palomar Observatory. Once implemented, this sensors will have superior performance to photon noise and low-spatial frequency phase errors than any other existing wavefront sensor.

## 9. ACKNOWLEDGEMENTS

This work was carried out by the Jet Propulsion Laboratory, California Institute of Technology, under contract with the National Aeronautics and Space Administration.

## REFERENCES

- [1] W. Linnik, "A simple interferometer to test optical systems," Proceedings of the Academy of Science of the USSR 1, 210-212 (1933).
- [2] F. Zernike, "Das Phasenkontrastverfahren bei der Mikroskopischen beobachtung," Z. Tech. Phys. **16**, 454 (1935).
- [3] F. Zernike, "Phasecontrast, a new method for the microscopic observation of transparent objects. Part I," Physica (Utrecht) **9** 686–698 (1942).
- [4] F. Zernike, "Phasecontrast, a new method for the microscopic observation of transparent objects. Part II.," Physica (Utrecht) **9**, 974–986 (1942).
- [5] F. Zernike, "How I discovered phase contrast," Science **121**, 345-349 (1955).
- [6] J. W. Goodman, *Introduction to Fourier Optics* (McGraw-Hill, 1996).
- [7] R. N. Smartt and W. H. Steel, "Theory and application of point-diffraction interferometers," Jpn. J. Appl. Phys. **14**, 351–356 (1975).
- [8] E. E. Bloemhof, J. K. Wallace, "Simple broadband implementation of a phase contrast wavefront sensor for adaptive optics", Optics Express **12**, 6240 – 6245 (2004).
- [9] M. A. Vorontsov, E. W. Justh, G. W. Carhart, L. A. Beresnev, Adaptive optics with advanced phase-contrast techniques. I. High-resolution wave-front sensing, J. Opt. Soc. Am. A **18**, 1289-1299 (2001).
- [10] E. W. Justh, M. A. Vorontsov, G. W. Carhart, L. A. Beresnev, and P. S. Krishnaprasad, "Adaptive optics with advanced phase-contrast techniques. II. High-resolution wave-front control," J. Opt. Soc. Am. A **18**, 1300–1311 (2001).
- [11] C. R. Mercer, K. Creath, "Liquid-crystal point-diffraction interferometer for wave-front measurements", Appl. Opt. **35**, pp. 1633, 1996
- [12] G. E. Sommargren and R. Hostetler, "Point diffraction interferometry at soft x-ray wavelengths," in *Soft X-Ray Projection Lithography*, A. M. Hawryluk and R. H. Stulen, eds., Vol. 18 of OSA Proceedings Series 1 Optical Society of America, Washington, D.C., 1993, p. 100
- [13] G. E. Sommargren, "Phase shifting diffraction interferometry for measuring extreme ultraviolet optics", OSA Trends in Optics and Photonics Vol. 4, Extreme Ultraviolet Lithography, G.D. Kubiak and D.R. Kania, eds. (Optical Society of America, Washington, DC 1996), pp. 108-112.
- [14] R. Soummer, et. al., "Fast computation of Lyot-style Coronagraph Propagation", Optics Express, **15**, 24 (2007).
- [15] O. Guyon, "Limits of Adaptive Optics for High Contrast Imaging", Astrophys. J. **629** (2005), 592-614
- [16] K. Dohlen, M. Langlois, P. Lanzoni, S. Mazzanti, A. Vigan, L. Montoya, E. Hernandez, M. Reyes, I. Surdej, N. Yaitskova, "ZEUS: a cophasing sensor based on the Zernike phase contrast method", Proc. SPIE **6267**, 626734 (2006).
- [17] T. Huang, W. Lu, S. Zhang, A. H. Greenaway, "Zernike Phase Sensor for phasing of segmented telescopes", Appl. Phys. B **86**, 139-145 (2007).
- [18] P. Ferraro, M. Paturzo and S. Grilli, "Optical wavefront measurement using a novel phase-shifting point-diffraction interferometer", SPIE

## BIOGRAPHY



**Kent Wallace** is a Senior Optical Engineer at the Jet Propulsion Laboratory. He has been involved in the design and development of several ground based instruments including the Palomar Testbed Interferometer, the Keck Interferometer and the Palomar Adaptive Optics System. His interest over the past few years has been nulling interferometry, optical communications, and wave front sensing. He has a BS in Physics from Rose-Hulman Institute of Technology (in beautiful, suburban Terre Haute, IN) and a MS in Optics from the University of Rochester.

